Accuracy of photocarrier radiometric measurement of electronic transport properties of ion-implanted silicon wafers

Bincheng Li[a)]
Center for Advanced Diffusion-Wave Technologies (CADIFT), Department of Mechanical and Industrial Engineering, University of Toronto, Toronto, Ontario, M5S 3G8, Canada and Photo-Thermal Diagnostics, Inc., 232 College Street, Toronto, Ontario, M5T 1R5, Canada

Derrick Shaughnessy
Center for Advanced Diffusion-Wave Technologies (CADIFT), Department of Mechanical and Industrial Engineering, University of Toronto, Toronto, Ontario, M5S 3G8, Canada

Andreas Mandelis[b)]
Center for Advanced Diffusion-Wave Technologies (CADIFT), Department of Mechanical and Industrial Engineering, University of Toronto, Toronto, Ontario, M5S 3G8, Canada and Photo-Thermal Diagnostics, Inc., 232 College Street, Toronto, Ontario, M5T 1R5, Canada

Jerias Batista
Center for Advanced Diffusion-Wave Technologies (CADIFT), Department of Mechanical and Industrial Engineering, University of Toronto, Toronto, Ontario, M5S 3G8, Canada

Jose Garcia
Photo-Thermal Diagnostics, Inc., 232 College Street, Toronto, Ontario, M5T 1R5, Canada

(Received 23 February 2004; accepted 6 April 2004)

The determination of the electronic transport properties of ion-implanted silicon wafers with the photocarrier radiometry (PCR) technique by fitting frequency scan data to a single layer model via a multiparameter fitting procedure is presented. A three-layer model is used to simulate the inhomogeneous structure of the ion-implanted wafers. The effects of the structural, electronic, and optical properties of the implanted layer, which are affected significantly by ion implantation, on the frequency behavior of the PCR signal of implanted wafers are discussed. Data simulated with the three-layer model are fitted to a single-layer model to extract the electronic transport properties of implanted wafers. The fitted carrier lifetime and diffusion coefficient are found to be close to that of the substrate layer which is assumed to remain intact after the ion implantation process. When self-normalized relative amplitude is used in the multiparameter fitting, the fitted surface recombination velocity is determined primarily by the level of electronic damage and is approximately independent of the level of optical damage. Experiments with boron implanted wafers were performed and the experimental results were in agreement with the simulations. These results show that the PCR technique is capable of measuring the bulk transport properties of ion-implanted silicon wafers. © *2004 American Institute of Physics.* [DOI: 10.1063/1.1755847]

I. INTRODUCTION

Among the physical parameters of semiconductors, the electronic transport properties, namely, the minority-carrier lifetime (τ), the carrier diffusion coefficient (D), and the (front and rear) surface recombination velocities (s_1 and s_2) have attracted great attention in semiconductor device manufacturing. Evaluation of these parameters is essential for characterizing semiconductor wafers, for defect and contamination monitoring, and for device modeling. The recently introduced technique of laser-induced infrared photocarrier radiometry (PCR) is a purely carrier-density-wave diagnostic method for noncontact characterization of the electronic transport properties of semiconductors.[1] It was derived from the well-known infrared photothermal radiometry (PTR), a technique extensively used in semiconductor characterization.[2–9] Both techniques rely on the detection of infrared emission from the semiconductor sample optically excited by an intensity-modulated laser beam with photon energy greater than the fundamental energy gap of the material. To simultaneously determine the transport properties, both the amplitude and phase of the PTR or PCR signal are recorded as a function of the modulation frequency over a wide range and then fitted with an appropriate theoretical model via a multiparameter fitting procedure. The uniqueness of the fitted results relies on the different effects of the individual parameters on the PCR signal.[10]

A common feature of the theoretical models used in the multiparameter fitting to extract the electronic transport properties of semiconductors is that in these models the semiconductors are assumed to be homogeneous samples with uniform properties. While this is generally true for non-implanted semiconductor wafers, a theoretical model with an

a)Present Address: Institute of Optics and Electronics, Chinese Academy of Sciences, P O Box 350 Shuangliu, Chengdu, Sichuan 610209, China; electronic mail: bcli@ioe.ac.cn
b)Electronic mail: mandelis@mie.utoronto.ca

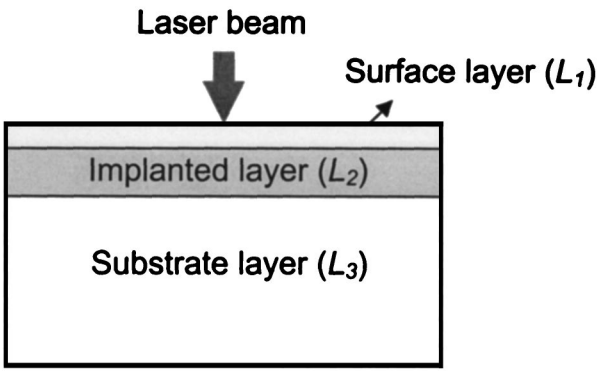

FIG. 1. Schematic diagram of the proposed three-layer structure of an ion-implanted silicon wafer.

assumed layered structure certainly better represents the actual structure of ion-implanted wafers. Therefore, to determine the transport properties of ion-implanted wafers, a model with layered structure should be used. However, difficulty arises because of the uniqueness issue with the multiparameter fitting procedure.[11] If a layered model is used in the fitting, a greater number of unknown parameters make the fitted results much less reliable. To obtain reliable fitting results with sufficient accuracy, only a few unknown parameters should be involved in the multiparameter fitting. A layered model therefore should be avoided in the fitting procedure.

To overcome this difficulty for the determination of the transport properties of ion-implanted wafers, the homogeneous layer model is still used in the fitting but the fitted results are discussed via a layered model to correlate the fitted values to the actual values of the transport properties of the ion-implanted wafers. Once the correlations between the fitted values extracted with the homogeneous layer model and the actual values of layered wafers are established, the transport properties of the ion-implanted (layered) wafers can be determined by fitting the PCR amplitude and phase to the single-layer model. In this article, a three-layer (a surface layer, an implanted layer, and a substrate layer) model is used to simulate the PCR signals of ion-implanted wafers. The simulated PCR amplitude and phase as a function of modulation frequency are then fitted via a least-squares process with a single-layer model to extract the effective transport properties of the ion-implanted wafers. The relationship between the extracted effective transport properties and the transport properties of the substrate layer and the effects of the optical and transport properties of the implanted layer (both the optical and the electronic transport properties of the implanted layer change with ion-implantation dose[12]) on the fitted transport properties are discussed.

II. THEORETICAL MODELS AND MULTIPARAMETER FITTING

The cross-section of an ion-implanted semiconductor wafer is schematically presented in Fig. 1. A three-layer structure is assumed: a surface layer, an ion-implanted layer, and a substrate layer. The surface layer represents a region traversed by the implanted ions. The ions do not reside within this region. The thickness of this upper layer depends on the implantation species and energy and is usually in the range of 0–100 nm when the energy is a few hundreds of keV or less. The second region lies within 10–500 nm below the surface of the wafer and represents the implanted layer where damage is maximum. The thickness of this implanted layer depends on both the implantation energy and the implantation dose. The third region is the remaining wafer and features transport and optical properties similar to the intact bulk wafer. The thicknesses of the three layers are denoted as L_1, L_2, and L_3, respectively.

The PCR detection geometry is the same as that for PTR of semiconductors.[6,7,9] The excitation beam is assumed to be Gaussian with a $(1/e)$-radius equal to a. The beam is modulated with an angular frequency ω $(\omega=2\pi f)$ and focused onto the ion-implanted side of a laterally semi-infinite semiconductor wafer. In PCR measurements, the thermal infrared (Planck-mediated) emissions are filtered out and only infrared (IR) emissions from the free-carrier wave component are detected by an appropriate IR detector and spectrally matched filter combination.[1] The PCR signal of an ion-implanted wafer is obtained by solving the carrier transport equations in the three regions and integrating the carrier density over the thickness of the whole wafer. By taking into account the collection efficiency of the IR detector, the PCR signal can be expressed as follows:[12]

$$S_{\mathrm{PCR}}(\omega)=C\int_0^\infty \tilde{F}(\delta,\omega)J_1(\delta w)\,d\delta, \tag{1}$$

with

$$\begin{aligned}\tilde{F}(\delta,\omega)=&\frac{1-\exp(-\beta_1 L_1)}{\beta_1}[A_1+B_1\exp(\beta_1 L_1)]\\&+\frac{E_1}{\alpha_1}[1-\exp(-\alpha_1 L_1)]\\&+\frac{1-\exp(-\beta_2 L_2)}{\beta_2}[A_2+B_2\exp(\beta_2 L_2)]\\&+\frac{E_2}{\alpha_2}[1-\exp(-\alpha_2 L_2)]\\&+\frac{1-\exp(-\beta_3 L_3)}{\beta_3}[A_3+B_3\exp(\beta_3 L_3)]\\&+\frac{E_3}{\alpha_3}[1-\exp(-\alpha_3 L_3)].\end{aligned} \tag{2}$$

C is a proportionality factor, J_1 represents the Bessel function of the first kind of order 1, w is the effective radius of the detector, and δ is the integration variable. A detailed description of the symbols used in Eq. (2) is given in Ref. 12 and is repeated in Appendix A. The single-layer model is obtained by simply assuming the thicknesses of the surface and implanted layers to be zero. It is also presented elsewhere[1,8] but the main expression is given in Appendix B. To determine the transport properties of semiconductor Si wafers, both the amplitude and the phase of the PCR signal

are measured as a function of modulation frequency in an appropriate frequency range and then fitted to an appropriate theoretical model.

To determine the electronic transport properties of ion-implanted wafers via a multiparameter fit to a single-layer model, the theoretical results of the three-layer model should be compared first to that of the single homogeneous layer model. In simulations, we first create a set of PCR data which include 32 amplitude points and 32 phase points in a modulation frequency range from 100 Hz to 1 MHz with the three-layer model. Then we perform a multiparameter fit of the simulated data to the single-layer model via a least-squares process to extract the effective transport properties of the ion-implanted (layered) Si wafers, namely, the carrier lifetime and diffusion coefficient, and the surface recombination velocities. Since ion implantation modifies mainly optical and electronic transport in the implanted layer, we discuss only the effects of the optical and electronic transport properties of the implanted layer on the fitted effective results of the ion-implanted wafers. In the multiparameter fitting process, the following square variance is minimized:

$$\mathrm{Var}=\frac{\Sigma_{m=1}^{N}[A^{T}(f_m)-A^{S}(f_m)]^2}{N}+\frac{\Sigma_{m=1}^{N}[\Phi^{T}(f_m)-\Phi^{S}(f_m)]^2}{\Sigma_{m=1}^{N}[\Phi^{S}(f_m)]^2}. \quad (3)$$

Here, $A^S(f_m)$ and $\Phi^S(f_m)$ are the PCR amplitude and phase simulated with the three-layer model and $A^T(f_m)$ and $\Phi^T(f_m)$ are the fitted PCR amplitude and phase calculated with the single-layer model. N is the total number of data points (32 in this case). During the fitting procedure, the three transport properties (τ, D, and s_1) and sometimes the absorption coefficient (α) in the single-layer model are set as free parameters. Either the absolute amplitude values or the relative amplitudes normalized by the value at the lowest frequency are used in the fitting. When the absolute values are used, the proportionality factor C is assumed to be known. Experimentally it can be determined by performing a ''calibration'' with a reference sample. The reference sample is usually a nonimplanted substrate wafer. When a reference sample is not available, a self-normalized amplitude can be used in the fitting. In this case, the PCR amplitude at the lowest frequency point simulated with the three-layer model and that calculated with the single-layer model are both normalized to 1 prior to fitting. By using the self-normalized amplitude in the fitting, the errors caused by a not-well-known reference are avoided.

III. SIMULATIONS

As stated before, since ion implantation affects significantly the implanted layer only, the effects of the properties of the implanted layer on the determination of the effective transport properties of the ion-implanted semiconductor wafer as a whole will be investigated exclusively, by discussing their impact on the frequency behavior of the PCR amplitude and phase. Since it is known that as the implantation dose increases electronic damage occurs before the onset of optical damage,[13,14] the effect of electronic damage on the frequency behavior is discussed first. Figure 2 shows the PCR amplitude and phase as a function of the modulation frequency for an ion-implanted semiconductor wafer at different levels of electronic damage caused by ion implantation, before the onset of optical damage. In the calculations, the carrier lifetime (τ_1), the diffusion coefficient (D_1), and the thickness (L_1) of the surface layer are assumed to be 0.5 μs, 3.5 cm^2/s, and 10 nm, respectively. The properties of the substrate layer (τ_3, D_3, and L_3) are assumed to be 5 μs, 35 cm^2/s, and 670 μm, respectively. Since optical damage does not yet appear (that is true when the implantation dose is low, say, below 10^{12} to $10^{14}\,\mathrm{cm}^{-2}$, depending on the type of implantation species[14]), the absorption coefficients ($\alpha_1, \alpha_2, \alpha_3$) of the three layers are assumed to be the same: $6.6\times10^4\,\mathrm{m}^{-1}$, which is the absorption coefficient of crystalline silicon (c-Si) at 830 nm wavelength. The thickness of the implanted layer is assumed to be 0.3 μm. In all cases the rear surface recombination velocity (s_2) is set to be 1.0×10^4 cm/s. Simulation results show that the PCR signal is not sensitive to s_2 in a wide range, from 100 to 1×10^6 cm/s. For the experimental parameters, the radius of the pump laser beam was measured by a pinhole scan and was found to be 25 μm. The effective size of the detector was determined to be 55 μm. The carrier lifetime and diffusion coefficient of the implanted layer are determined by the electronic damage level through the effective medium approximation,[14–16] with the lifetimes and diffusion coefficients of perfectly crystalline and totally electronically damaged silicon wafers assumed to be 5 μs and 1 ns, and 35 and

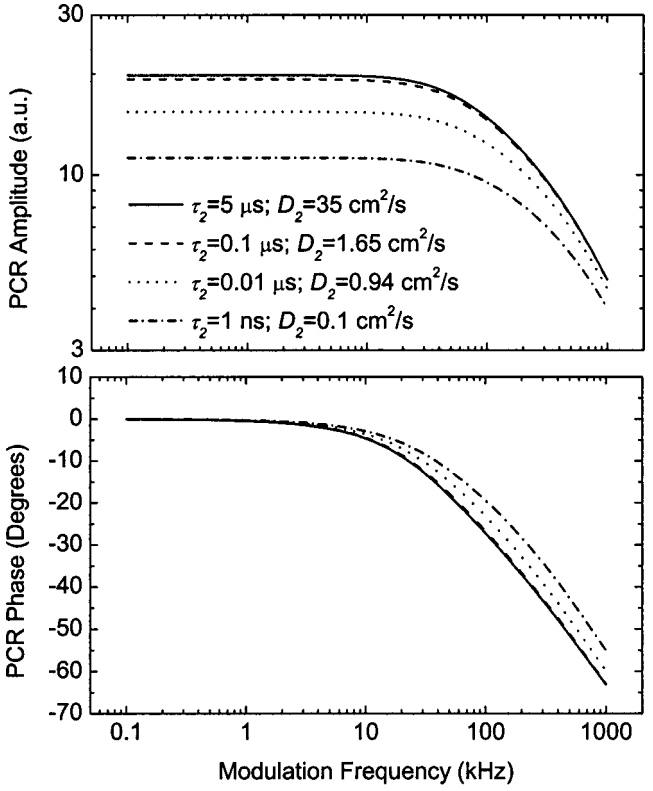

FIG. 2. Frequency dependence of PCR amplitude and phase with various levels of electronic damage in the implanted layer.

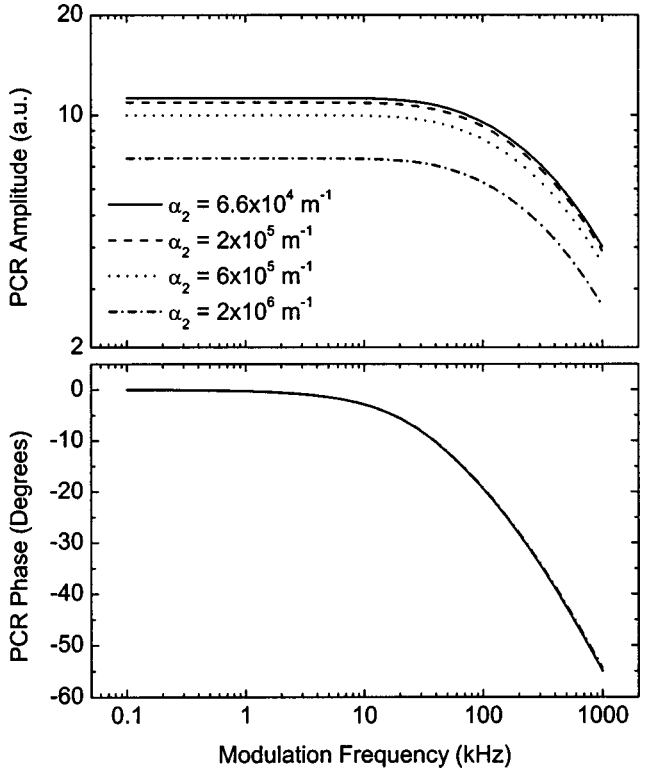

FIG. 3. Frequency dependence of PCR amplitude and phase with various levels of optical damage and total electronic damage in the implanted layer. The electronic transport properties of the implanted layer are the same as that of a-Si: $\tau_2 = 1$ ns, $D_2 = 0.1$ cm^2/s.

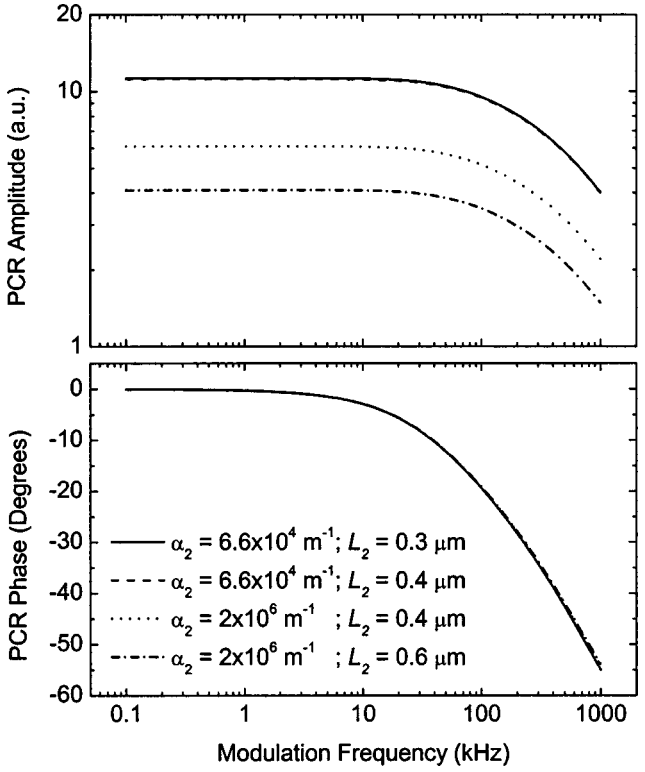

FIG. 4. Frequency dependence of PCR amplitude and phase with various levels of optical damage, different thickness, and total electronic damage in the implanted layer, as in Fig. 3.

0.1 cm^2/s, respectively. The increased electronic damage level causes the PCR amplitude to decrease and the turning frequency where the PCR amplitude begins decreasing moves to higher values, a phenomenon consistent with the effect of increasing front surface recombination velocity on the frequency behavior.[10]

As the implantation dose increases, optical damage occurs in the implanted layer, in addition to a total electronic damage. The optical damage causes the absorption coefficient of the implanted layer to increase, until it is totally saturated to the absorption coefficient of amorphous silicon (a-Si). At 830 nm, the absorption coefficient of a-Si is approximately $2.0\times10^6\,\mathrm{m}^{-1}$,[17] about 30 times that of c-Si. Figure 3 shows the influence of the increasing level of optical damage on the frequency behavior of the PCR signal. The PCR amplitude decreases with increasing absorption coefficient (increasing damage level). However, the shape of the frequency curve of the PCR amplitude and the PCR phase are approximately independent of the absorption coefficient. The increasing absorption coefficient causes an approximately equal drop of the amplitude in the whole frequency range. An increase in the thickness of the implanted layer causes a similar effect on the frequency behavior of PCR amplitude and phase, as presented in Fig. 4. That is, the PCR amplitude decreases with increasing thickness, and the PCR phase is approximately independent of the thickness.

The simulated data presented in Figs. 2–4 are now fitted to the single-layer model and the corresponding best fits are presented in Figs. 5–7. Figure 5 shows the best fits to the

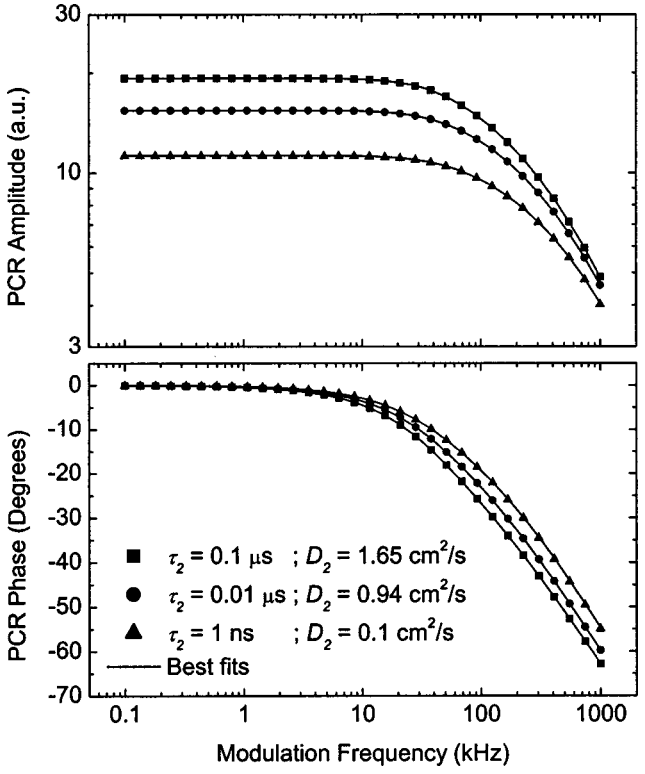

FIG. 5. Best fits (solid lines) to the simulated frequency dependence (symbols) of PCR amplitude and phase with various levels of electronic damage in the implanted layer.

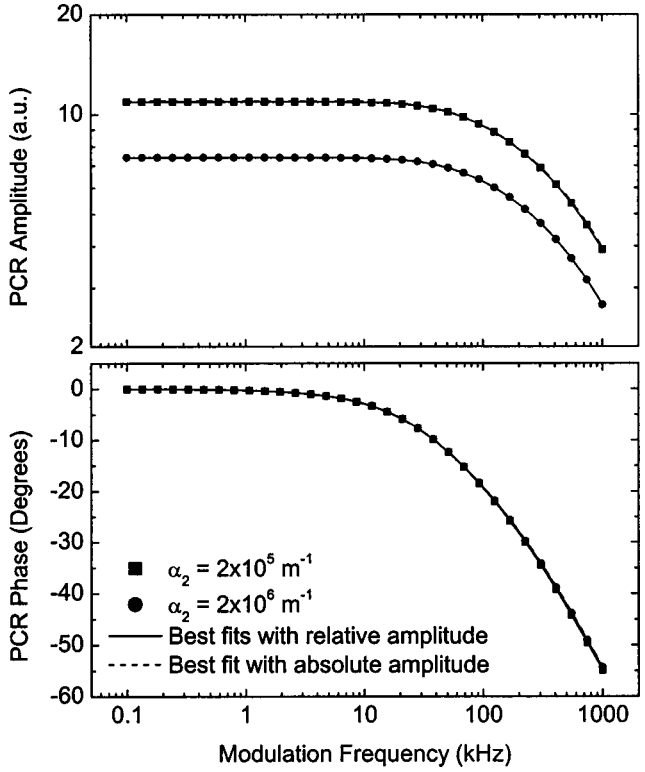

FIG. 6. Best fits (lines) to the simulated frequency dependence (symbols) of PCR amplitude and phase with two different levels of optical damage in the implanted layer. Solid lines represent the fits with the self-normalized amplitude and the dashed line represents the best fit with the absolute amplitude and absorption coefficient of $2\times10^5\ m^{-1}$. (Dashed line is not visible).

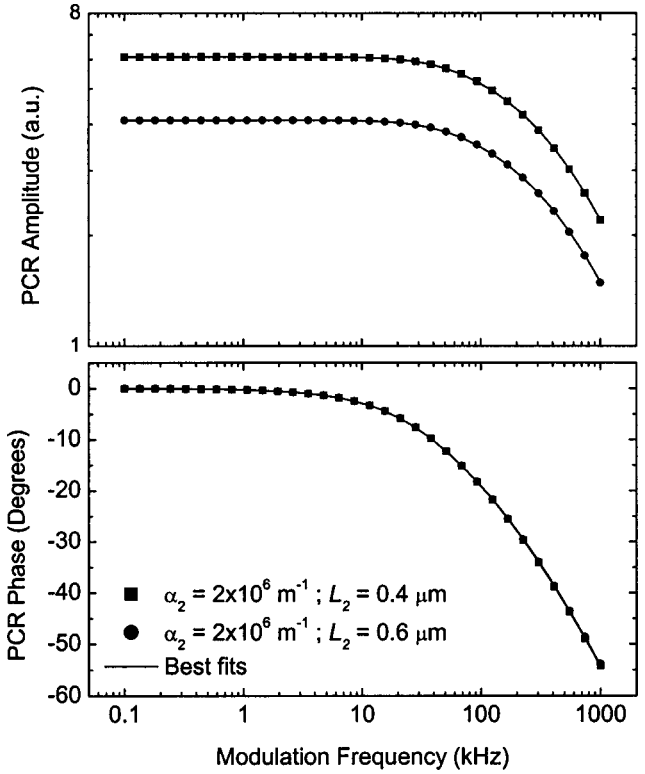

FIG. 7. Best fits (solid lines) to the simulated frequency dependence (symbols) of PCR amplitude and phase with different thicknesses of the implanted layer. The implanted layer was totally damaged both electronically and optically. With complete damage, the optical and electronic transport properties of the implanted layer are the same as that of a-Si: $\alpha_2=2\times10^6\ m^{-1}$, $\tau_2=1$ ns, and $D_2=0.1\ cm^2/s$.

simulated data presented in Fig. 2 and represents the influence of the electronic damage on the frequency behavior of the PCR signal. The absolute amplitude values are used in the fitting. The diffusion coefficient and absorption coefficient are fixed to the values of c-Si, while the carrier lifetime and front surface recombination velocity are set as free parameters to minimize the square variance. The fitted results are presented in Table I, together with fitted results obtained with free D and/or self-normalized amplitude. In all cases the square variance is well below that due to the experimental error, estimated to be between 0.001 and 0.0001 therefore all fitted results are considered acceptable. From Table I, the fitted effective front surface recombination velocity increases with increasing electronic damage rate. In all cases the fitted effective carrier lifetime of the implanted wafer is close to the lifetime of the substrate layer (within 4% maximum) and the fitted effective diffusion coefficient is close to the diffusion coefficient of the substrate layer (the difference is less than 10% in the worst case) if the diffusion coefficient is also set as a free parameter. Since the implanted layer lies close to the surface, the effect of the electronic damage in the implanted layer on the PCR signal is approximately equivalent to that of changed surface recombination. It is also noticed that the effective transport properties fitted with either the absolute amplitude or self-normalized amplitude are close to each other. However, when the self-normalized amplitude is used in the fitting, the square variance is much lower when the electronic damage rate is high, and the fitted lifetime and diffusion coefficient are closer to that of the substrate layer (within 1%). These results reflect the fact that with an optical penetration depth of 15 μm (at 830 nm), the PCR signal is dominated by the contribution of the substrate layer.

Figure 6 shows the best fits when optical damage is also present. Two different levels of optical damage are assumed and fitted in the figure. In all cases, a total electronic damage is assumed, considering the fact that electronic damage becomes saturated when optical damage begins. The electronic transport properties of the implanted layer are therefore assumed to be the same as those of a-Si. With moderate optical damage rate, both the absolute and the self-normalized amplitudes are used in the fitting. When the optical damage level is high, only the self-normalized amplitude is used because if the absolute amplitude is used, the square variance is too high and the fitted results cannot be considered as acceptable. The fitted results are summarized in Table II with two to four free parameters set in the multiparameter fitting. When the absolute amplitude is used in the fitting, the square variance is high (larger than 0.0001) if both the diffusion coefficient and absorption are fixed to the values of the substrate layer. Also, the fitted effective lifetime is well above the lifetime of the substrate layer with the error increasing with increasing level of optical damage. If the diffusion coefficient is fixed but the absorption coefficient is set as a free parameter, the square variance is about one order of magnitude lower and the fitted results are less erroneous. If both

TABLE I. Fitted results for simulated data with various electronic damage rates.

Amplitude used in the fitting and other assumptions	Input τ_2 and D_2 (μs and cm^2/s)	Fitted lifetime (τ) (μs)	Fitted D (cm^2/s)	Fitted s_1 (cm/s)	Square variance
Absolute amplitude	0.1:1.65	4.92	35.0 (fixed)	1215	7.69×10^{-7}
	0.01:0.94	4.95	35.0 (fixed)	3754	2.2×10^{-7}
Fix D	0.001:0.1	5.14	35.0 (fixed)	10468	2.24×10^{-5}
Absolute amplitude	0.1:1.65	5.04	34.6	1329	1.97×10^{-7}
	0.01:0.94	5.01	34.7	3850	2.2×10^{-7}
Free D	0.001:0.1	5.18	31.8	12091	1.56×10^{-6}
Self-normalized amplitude	0.1:1.65	4.95	35.0 (fixed)	1240	2.8×10^{-7}
	0.01:0.94	4.97	35.0 (fixed)	3770	1.3×10^{-7}
Fix D	0.001:0.1	5.01	35.0 (fixed)	10020	3.64×10^{-9}
Self-normalized amplitude	0.1:1.65	5.03	34.7	1318	1.13×10^{-8}
	0.01:0.94	5.01	34.7	3858	5.65×10^{-9}
Free D	0.001:0.1	5.0	35.1	9968	1.42×10^{-9}

the diffusion coefficient and absorption coefficient are set as free parameters, the fitting error further improves. In both cases the fitted front surface recombination velocity and absorption coefficient are not reliable due to the close correlation of their effects on the PCR signal. However, if the self-normalized amplitude is used in the fitting instead, the fitted lifetime and diffusion coefficient (if it is set as a free parameter) are close to that of the substrate layer (within 3% and 4%, respectively). The fitted front surface recombination velocity is approximately independent of the level of optical damage. In the case where both the diffusion coefficient and absorption coefficient are set as free parameters, the fitted diffusion coefficient decreases slightly and the fitted absorption coefficient increases with increasing level of optical

TABLE II. Fitted results for simulated data with various optical damage rates.

Amplitude used and other assumptions	Input α_2 (m^{-1})	Fitted lifetime (τ) (μs)	Fitted D (cm^2/s)	Fitted α (m^{-1})	Fitted s_1 (cm/s)	Square variance
Absolute amplitude	2×10^5	5.49	35.0 (fixed)	6.6×10^4 (fixed)	1.16×10^4	2.38×10^{-4}
	6×10^5	6.68	35.0 (fixed)	6.6×10^4 (fixed)	1.58×10^4	2.04×10^{-3}
Fixed D and α	2×10^6	13.36	35.0 (fixed)	6.6×10^4 (fixed)	4.93×10^4	1.45×10^{-2}
Absolute amplitude	2×10^5	4.68	35.0 (fixed)	1.65×10^5	7800	9.91×10^{-6}
Fixed D, free α	6×10^5	4.61	35.0 (fixed)	4.45×10^9	7400	2.64×10^{-5}
	2×10^6	8.35	35.0 (fixed)	3.89×10^4	6.05×10^8	6.14×10^{-3}
Absolute amplitude	2×10^5	4.92	32.1	1.31×10^5	9176	2.35×10^{-6}
	6×10^5	4.92	23.1	1.05×10^5	1.40×10^4	1.55×10^{-5}
Free D and α	2×10^6	4.37	18.6	7.55×10^4	4.06×10^6	1.50×10^{-4}
Self-normalized amplitude	2×10^5	5.01	35.0 (fixed)	6.6×10^4 (fixed)	1.01×10^4	2.91×10^{-8}
	6×10^5	5.05	35.0 (fixed)	6.6×10^4 (fixed)	1.03×10^4	2.55×10^{-7}
Fixed D and α	2×10^6	5.16	35.0 (fixed)	6.6×10^4 (fixed)	1.10×10^4	3.11×10^{-6}
Self-normalized amplitude	2×10^5	4.99	35.1	6.81×10^4	9878	1.99×10^{-9}
	6×10^5	4.99	34.5	7.88×10^4	9702	8.13×10^{-10}
Free D and α	2×10^6	4.99	33.6	1.18×10^5	9429	6.40×10^{-9}

TABLE III. Fitted results for simulated data with varying thickness of implanted layer.

Amplitude used and other assumptions	Input L_2 and α_2 (μm and m^{-1})	Fitted lifetime (τ) (μs)	Fitted D (cm^2/s)	Fitted α (m^{-1})	Fitted s_1 (cm/s)	Square variance
Absolute amplitude	$0.4{:}6.6\times10^4$	5.22	35.0 (fixed)	6.6×10^4 (fixed)	1.07×10^4	5.16×10^{-5}
Fixed D and α						
Absolute amplitude	$0.4{:}6.6\times10^4$	4.82	35.0 (fixed)	1.03×10^5	8541	3.07×10^{-6}
Fixed D, free α						
Absolute amplitude	$0.4{:}6.6\times10^4$	5.01	32.7	8.81×10^4	9995	1.43×10^{-7}
Free D and α	$0.4{:}2\times10^6$	3.78	14.3	1.23×10^5	5.60×10^7	5.44×10^{-4}
	$0.6{:}2\times10^6$	2.93	9.42	2.65×10^5	8.12×10^7	2.16×10^{-3}
Self-normalized amplitude	$0.4{:}6.6\times10^4$	5.01	35.0 (fixed)	6.6×10^4 (fixed)	1.01×10^4	5.12×10^{-9}
	$0.4{:}2\times10^6$	5.21	35.0 (fixed)	6.6×10^4 (fixed)	1.12×10^4	5.62×10^{-6}
Fixed D and α	$0.6{:}2\times10^6$	5.35	35.0 (fixed)	6.6×10^4 (fixed)	1.18×10^4	1.60×10^{-5}
Self-normalized amplitude	$0.4{:}6.6\times10^4$	5.00	35.0	6.68×10^4	9978	7.36×10^{-10}
	$0.4{:}2\times10^6$	4.99	33.1	1.47×10^5	9381	1.69×10^{-8}
Free D and α	$0.6{:}2\times10^6$	4.90	35.4	2.15×10^5	8463	5.77×10^{-7}

damage. Overall, when the self-normalized amplitude is used, the fitted results are close to that without optical damage. This is so because optical damage causes mainly the PCR amplitude to decrease equally over the whole frequency range, but does not alter the shapes of the frequency dependencies of PCR amplitude and phase.

Figure 7 shows the best fits with a different degree of optical damage from Fig. 6 and with different thicknesses of the implanted layer. The fitted results are presented in Table III. Good fits are obtained when the self-normalized amplitude is used in the fitting. This is because the increase in the thickness of the implanted layer causes mainly a decline of the PCR amplitude, which does not affect significantly the frequency behavior of the PCR signal, as shown in Fig. 4.

In summary, simulation results prove that ion-implanted wafers can be treated as a homogeneous layer sample with modified electronic transport properties. Because the absorption coefficient and thickness of the implanted layer affect primarily only the amplitude, and only slightly the frequency behavior or the phase of the PCR signal, and the effect of the lifetime and diffusion coefficient of the implanted layer on the frequency behavior of the PCR signal can be included in a modified front surface recombination velocity, the lifetime and diffusion coefficient of the substrate wafer can be determined by fitting the experimental data of implanted wafers to a single-layer model via a multiparameter fitting procedure. In all cases if the self-normalized amplitude is used in the fitting, the extracted lifetime and diffusion coefficient are close to that of the substrate layer, and the extracted front surface recombination velocity is determined by the level of electronic damage in the implanted layer. If the absolute amplitude is used in the fitting, the substrate lifetime and diffusion coefficient can still be extracted with sufficient accuracy if the level of optical damage is low or moderate, with optical damage rate[12] less than 0.6.

IV. EXPERIMENTAL RESULTS AND DISCUSSION

Experiments with several industrial Si wafers were performed to verify the theoretical simulations presented above. The experimental setup has been described in detail elsewhere.[1,18] Briefly, a tunable Ti: sapphire laser pumped by a 10-W 532 nm laser was used as the excitation source. The laser was operated at 830 nm wavelength and the power of the beam was 22.8 mW. The laser beam was focused onto the sample surface and the radius of the beam at the surface was measured to be approximately 25 μm. The infrared emission from the sample was collected and focused through a pair of reflective objectives onto an InGaAs detector, preamplifier, and optical cut-on filter assembly. The effective radius of the detector was estimated to be 55 μm. The spectral response range of the detector optics was 0.8–1.8 μm. The spectrally matched filter further served to block any leakage of the excitation source. The samples used in the experiments were (100) oriented *p*-type silicon wafers, 10–20 Ω cm, implanted with $^{11}B^+$ at an energy of 50 keV. The thicknesses of these wafers were 675 ± 20 μm. The wafers were implanted at room temperature at an angle of 7° to suppress channeling with doses from 1×10^{10} to $1\times10^{16}\,cm^{-2}$.

For each silicon wafer, the PCR signal was recorded as a function of modulation frequency with two lock-in amplifiers (LIA). The first LIA (SRS Model SR850) recorded the PCR signal from 100 Hz to 100 kHz and the second one (SRS Model SR844) recorded the signal from 100 kHz to 1 MHz. Together the amplitude and phase of the PCR signal were recorded at a total of 32 frequency points spanning from 100 Hz to 1 MHz. To eliminate the influence of instrumental transfer function, the amplitude and phase of the PCR signal were normalized by the detector signal recorded with the scattering light of the excitation beam (in this case the filter in front of the detector was removed). After normalization,

the amplitudes and phases recorded with the two LIAs were merged in the overlapping frequency range (around 100 kHz).

A high-quality nonimplanted silicon wafer from the same batch as the implanted wafers was first measured to determine the proportionality factor C in Eq. (1) and the diffusion coefficient of the substrate layer of implanted wafers, assuming they have the same diffusion coefficient. The lifetime of this high-quality nonimplanted wafer was supposed to be on the order of 1 ms. In this case the exact value is not important as the PCR signal is insensitive to lifetime within the chosen frequency range f higher than 100 Hz, as long as the lifetime is higher than a certain value, typically 0.2 ms. By setting the diffusion coefficient, the front surface recombination velocity, and the effective detector size as free parameters, the experimental data of the nonimplanted wafer were fitted to the homogeneous layer model. In the fitting, the rear surface recombination velocity was assumed to be 1×10^4 cm/s. However, the exact value is not important as mentioned above. The beam radius was determined to be 25 μm, measured by scanning a pinhole. The fitted diffusion coefficient was approximately 35 cm^2/s, which is close to that of the monority carriers in a typical p-type wafers.[19] The fitted front surface recombination velocity was 385 cm/s, which is within the typical range for nonimplanted wafers.[20] The effective detector radius was determined to be 55 μm. The experimental data of the implanted wafers were then fitted to the homogeneous layer model to determine the lifetime and the effective front surface recombination velocity of the wafers implanted with different doses. In the fitting, the diffusion coefficient was fixed to 35 cm^2/s, determined with the nonimplanted wafer. The absorption coefficient was not set as a free parameter, as it was found out that the effects of the surface recombination velocity and of the absorption coefficient on the PCR signal are closely correlated and both parameters could not be determined simultaneously via a multiparameter fitting procedure. It was not set to the absorption coefficient of c-Si either: Experimentally it was found that, with the exception of the lowest dose, the fits were not acceptable if the absorption coefficient of c-Si was assumed. The fits were acceptable and the square variance became insensitive to the absorption coefficient only when the latter was higher than a certain value (around $2\times10^5\ m^{-1}$). Several absorption coefficient values were therefore used for each wafer and the influence of the absorption coefficient was investigated (see below). For our fitting procedure, the lifetime and front surface recombination velocity were set as free parameters to minimize the square variance. Both the absolute and self-normalized amplitudes were used in the fitting. The fitted square variance was between 0.0002 and 0.009. This relatively high square variance is due to the relatively high measurement error in PCR phase at the high frequency end.

The experimental data and the corresponding best fits are presented in Fig. 8 and the fitted lifetime and front surface recombination velocity are shown in Fig. 9, together with the assumed absorption coefficient values. Figure 9(a) shows the assumed absorption coefficient. For each sample with a different dose, three or four absorption coefficient values were assumed and are represented by solid squares. The empty circle represents the absorption coefficient of c-Si. The dashed line represents a polynomial fit of all discrete points. The best fits presented in Fig. 8 were obtained with the assumed absorption coefficient at each dose being closest to the polynomial fit and using absolute amplitude. Solid squares in Fig. 9(b) represent the fitted lifetime. For each sample, three or four fitted values are presented, corresponding to the three or four assumed absorption coefficient values in Fig. 9(a). With the exception of the lowest dose sample, the fitted lifetime values with different absorption coefficients are very close to each other and cannot be separated in the figure, indicating that the fitted lifetime is approximately independent of the assumed absorption coefficient, as expected from the theoretical predictions. The empty circle at the lowest dose represents the fitted lifetime when the absorption coefficient of the sample was assumed to be that of c-Si. From Fig. 9(b), when the absolute amplitude was used in the fitting, the fitted lifetime was approximately independent of the implantation dose (within experimental error) except for the $10^{10}\ cm^{-2}$ dose. The higher lifetime values of the 10^{15} and $10^{16}\ cm^{-2}$ doses are due to a lower signal-to-noise ratio as the amplitude levels are lower at the high dose end. Higher lifetime was also obtained for the lowest dose wafer. The reason is not clear. The fitted lifetime for the lowest dose is approximately 13 μs and the average lifetime for the higher dose wafers is approximately 4 μs. It was also noticed that the fitted lifetime of implanted wafers was substantially lower than that of the corresponding nonimplanted wafer. One possibility for these observations is that at 830 nm with

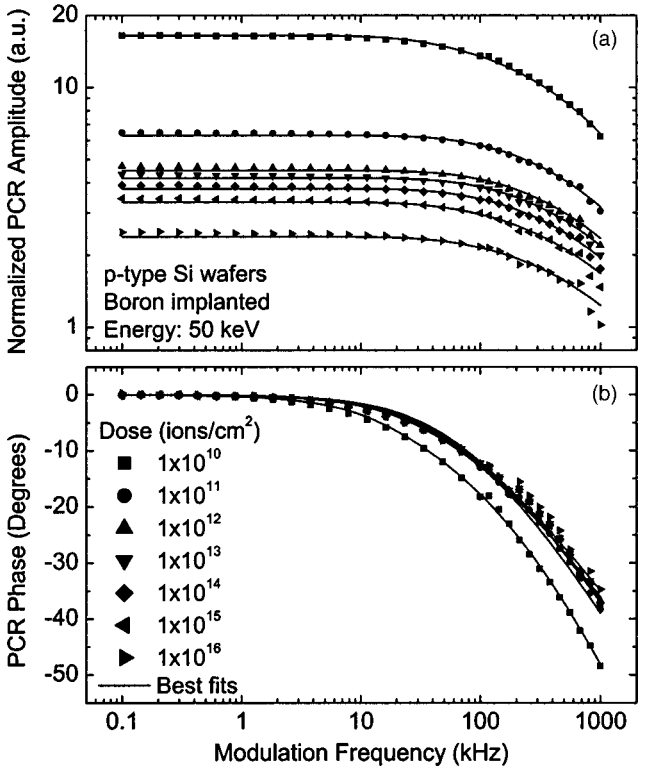

FIG. 8. Experimental frequency dependence of PCR amplitude and phase and the corresponding best fits. The samples were boron implanted p-type silicon wafers with doses from 10^{10} to $10^{16}\ cm^{-2}$. The implantation energy was 50 keV.

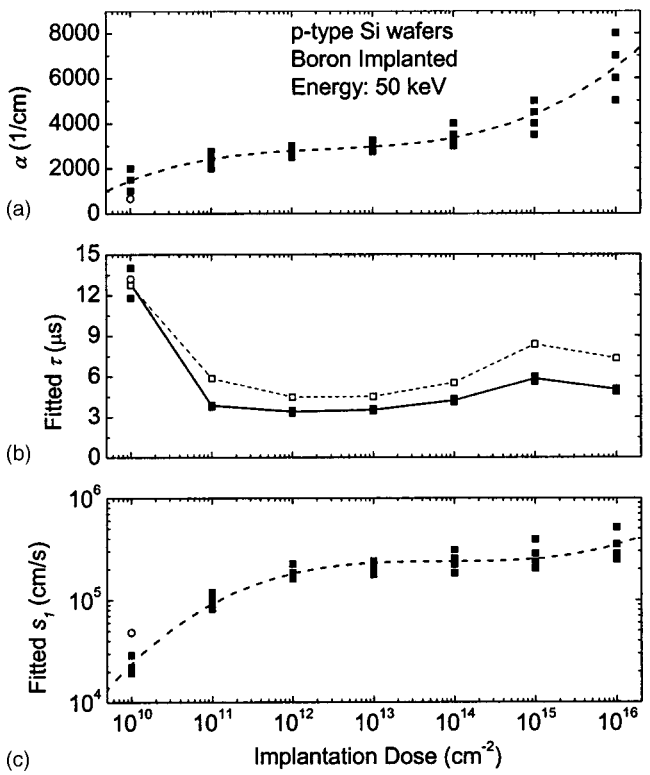

FIG. 9. The assumed absorption coefficient (a), the fitted carrier lifetime (b), and the fitted front surface recombination velocity (c) as functions of implantation dose. The samples were boron implanted *p*-type silicon wafers with doses from 10^{10} to $10^{16}\,cm^{-2}$. The implantation energy was 50 keV. The dashed lines in (a) and (c) are polynomial fits to guide the eye. The solid squares in (a) represent the assumed absorption coefficient values. For each sample, three or four absorption coefficient values were assumed, as shown by the vertical squares at each dose. The solid squares and solid line in (b) represent the results obtained with the absolute amplitude and the empty squares and dotted line represent the results obtained with the self-normalized amplitude. The solid squares in (c) represent the fitted recombination velocities corresponding to the assumed absorption coefficient values. The open circles in (a), (b), and (c) represent the absorption coefficient of *c*-Si and corresponding fitted lifetime and recombination velocity.

optical absorption length α^{-1} equal to $\sim 2.5\ \mu m$, instead of the true bulk lifetime, PCR is measuring the effective lifetime[21] which has contributions from both surface and bulk. The surface lifetime is a strong function of the surface recombination velocity. Therefore, unlike time-domain techniques,[22] the ability to measure S_1 independently with frequency-domain PCR allows, in principle, the unique determination of both surface and bulk lifetimes. Figure 9(c) presents the fitted front surface recombination velocity. For each sample, three or four values were obtained, corresponding to the assumed absorption coefficient values. The fitted recombination velocity at each dose is sensitive to the assumed absorption coefficient for that dose. The highest fitted recombination velocity value *for a given dose* corresponds to the lowest assumed absorption coefficient for the dose and the fitted recombination velocity decreases monotonically with the assumed increasing absorption coefficient for each dose. This is so because for a given sample, the effect of surface recombination on the PCR signal is determined by both the recombination velocity and the surface carrier density. The latter, in turn, increases with an increasing absorption coefficient due to the increased optical density. Therefore, the contribution of an increased recombination velocity to the overall effects of surface recombination on the PCR signal can be compensated (at least partially) by the contribution of a decreased absorption coefficient. From Fig. 9(c), the fitted surface recombination velocity increases with increasing dose, which is in agreement with the simulation results presented in the last section. When the self-normalized amplitude was used in the fitting, the fitted lifetimes were somewhat higher than that obtained when the absolute amplitude was used. However, its dependence on the implantation dose is similar to that obtained with the absolute amplitude. The fitted lifetime for the lowest dose is approximately 12 μs and the average lifetime for higher dose wafers is approximately 5 μs. The fitted surface recombination velocity was basically saturated at the 10^6–10^7 cm/s level, independent of the implantation dose, except at the lowest dose (not shown in the figure), in agreement with the simulation results. The fitted recombination velocity values were less reliable than that obtained when the absolute amplitude was used due to the fact that the fitted recombination velocity is more sensitive to the error in phase measurement at the high frequency end.

It is worth noting that there is a large difference between the lifetime of the implanted wafers and that of the nonimplanted wafer, that is, the measured lifetime of a highly implanted wafer is much lower than that of the corresponding nonimplanted wafer, while at low dose, the lifetime is somewhere in between. From the simulations it is clear that the fitted lifetime of implanted wafers represents that of the substrate layer, which was assumed not to be affected by ion implantation. The experimental results do indicate that ion implantation does affect the transport properties of the substrate layer, probably due to ion or defect diffusion deep into the substrate, even though the effect is much less significant than that on the implanted layer.

V. CONCLUSIONS

Simulations have been performed to investigate the accuracy of the determination of the electronic transport properties of implanted silicon wafers with photocarrier radiometry by fitting frequency scan data to a single layer model via a multiparameter fitting procedure. A three-layer model was used to simulate the inhomogeneous structure of the ion-implanted wafers. The effects of the structural, electronic, and optical properties of the implanted layer on the frequency behavior of the PCR signal of implanted wafers were discussed in detail. Data simulated with the three-layer model were fitted to a single-layer model to extract the electronic transport properties of implanted wafers. The fitted lifetime and diffusion coefficient were found to be close to that of the substrate layer which was assumed to remain intact by the ion implantation process. If the absolute amplitude is used in the multiparameter fit, the fitted front surface recombination velocity becomes a complicated function of the structural, optical, and transport properties of the implanted layer and the fitted value is subject to how accurately the optical properties of the implanted wafer are known. The

fitting error increases significantly when optical damage is present. The absolute amplitude should be used only if the optical damage is low to moderate. However, if the self-normalized amplitude is used in the fitting instead, the fitted lifetime and diffusion coefficient are very close to that of the substrate layer and the fitted recombination velocity is determined by the level of electronic damage, and is approximately independent of the level of optical damage. Experiments with boron implanted wafers were performed and the experimental results were in agreement with the simulations. Both types of results with conventional (absolute) normalization and self-normalization confirmed that the PCR technique is capable of measuring the electronic transport properties of ion-implanted wafers.

ACKNOWLEDGMENTS

The financial support of Materials and Manufacturing Ontario (MMO) through a Collaborative Contract to A.M. and of the Natural Science and Engineering Council of Canada (NSERC) is gratefully acknowledged.

APPENDIX A: SYMBOL DEFINITIONS APPEARING IN EQ. (2)

$$\beta_n^2=\delta^2+\sigma_n^2, \quad (n=1,2,3) \tag{A1}$$

$$\sigma_n^2=\frac{1+i\omega\tau_n}{D_n\tau_n}, \quad (n=1,2,3) \tag{A2}$$

$$E_1=\frac{\alpha_1(1-R_1)\eta P}{2\pi h\nu D_1}\frac{\exp(-\delta^2a^2/4)}{\beta_1^2-\alpha_1^2}, \tag{A3}$$

$$E_2=\frac{\alpha_2(1-R_1)(1-R_2)\eta P}{2\pi h\nu D_2}\frac{\exp(-\delta^2a^2/4-\alpha_1L_1)}{\beta_2^2-\alpha_2^2}, \tag{A4}$$

$$E_3=\frac{\alpha_3(1-R_1)(1-R_2)(1-R_3)\eta P}{2\pi h\nu D_3}\times\frac{\exp(-\delta^2a^2/4-\alpha_1L_1-\alpha_2L_2)}{\beta_3^2-\alpha_3^2}, \tag{A5}$$

$$A_1=\frac{1}{H}\left\{-\left[\frac{b_1}{a_1}(a_2+p_2g_1)\exp(\beta_1L_1)-(b_2-p_2g_1)\times\exp(-\alpha_1L_1)\right]E_1+[p_2g_1(1+\gamma_2)+(g_1\gamma_2-h_2)]E_2+\frac{2g_1\gamma_3}{1+\gamma_1}E_3\right\}, \tag{A6}$$

$$B_1=\frac{1}{a_1H}\left\{-[b_1(1-p_2g_1)\exp(-\beta_1L_1)-(b_2-p_2g_1)\exp(-\alpha_1L_1)]E_1+[p_2g_1(1+\gamma_2)+(g_1\gamma_2-h_2)]E_2+\frac{2g_1\gamma_3}{1+\gamma_1}E_3\right\}, \tag{A7}$$

$$H=\frac{1}{a_1}(a_2+p_2g_1)\exp(\beta_1L_1)-(1-p_2g_1)\times\exp(-\beta_1L_1); \tag{A8}$$

$$A_2=\frac{1}{2g_1}[(1+g_1)A_1\exp(-\beta_1L_1)+(g_1-a_2)B_1\exp(\beta_1L_1)+(g_1+b_2)E_1\times\exp(-\alpha_1L_1)-(g_1+h_1)E_2], \tag{A9}$$

$$B_2=\gamma_1A_2+\gamma_2E_2+\gamma_3E_3; \tag{A10}$$

$$A_3=\frac{1}{2g_2}[(1+g_2)A_2\exp(-\beta_2L_2)+(g_2-a_3)B_2\exp(\beta_2L_2)+(g_2+b_3)E_2\times\exp(-\alpha_2L_2)-(g_2+h_2)E_3] \tag{A11}$$

$$B_3=\mu A_3+\gamma E_3; \tag{A12}$$

with

$$a_1=\frac{D_1\beta_1-s_1}{D_1\beta_1+s_1}, \tag{A13}$$

$$b_1=\frac{D_1\alpha_1+s_1}{D_1\beta_1+s_1}, \tag{A14}$$

$$a_2=\frac{D_1\beta_1+s_2}{D_1\beta_1-s_2}, \tag{A15}$$

$$b_2=\frac{D_1\alpha_1-s_2}{D_1\beta_1-s_2}, \tag{A16}$$

$$a_3=\frac{D_2\beta_2+s_3}{D_2\beta_2-s_3}, \tag{A17}$$

$$b_3=\frac{D_2\alpha_2-s_3}{D_2\beta_2-s_3}, \tag{A18}$$

$$a_4=\frac{D_3\beta_3+s_4}{D_3\beta_3-s_4}, \tag{A19}$$

$$b_4=\frac{D_3\alpha_3-s_4}{D_3\beta_3-s_4}, \tag{A20}$$

$$g_1=\frac{D_2\beta_2}{D_1\beta_1-s_2}, \tag{A21}$$

$$g_2=\frac{D_3\beta_3}{D_2\beta_2-s_3}, \tag{A22}$$

$$h_1=\frac{D_2\alpha_2}{D_1\beta_1-s_2}, \tag{A23}$$

$$h_2=\frac{D_3\alpha_3}{D_2\beta_2-s_3}, \tag{A24}$$

$$\mu=\frac{1}{a_4}\exp(-2\beta_3L_3), \tag{A25}$$

$$\gamma=\frac{b_4}{a_4}\exp(-\beta_3 L_3-\alpha_3 L_3), \tag{A26}$$

$$p_1=\frac{1-\mu}{1+\mu}, \tag{A27}$$

$$\gamma_1=\frac{1-p_1 g_2}{a_3+p_1 g_2}\exp(-2\beta_2 L_2), \tag{A28}$$

$$\gamma_2=\frac{b_3-p_1 g_2}{a_3+p_1 g_2}\exp(-\beta_2 L_2-\alpha_2 L_2), \tag{A29}$$

$$\gamma_3=\frac{p_1 g_2(1+\gamma)+g_2\gamma-h_2}{a_3+p_1 g_2}\exp(-\beta_2 L_2), \tag{A30}$$

$$p_2=\frac{1-\gamma_1}{1+\gamma_1}. \tag{A31}$$

Here, D_n and $\tau_n\,(n=1,2,3)$ are the minority (electron) carrier diffusion coefficient and lifetime of the surface layer, implanted layer, and substrate layer, respectively. α_1, α_2, and α_3 are their absorption coefficients, respectively. L_1, L_2, and L_3, are the thicknesses of the three layers, respectively, a is the $(1/e)$-radius of the Gaussian excitation beam and $\omega\,(\omega=2\pi f)$ is the angular modulation frequency of the beam. s_1 and s_4 are the front and rear surface recombination velocities of the wafer, and s_2 and s_3 are the effective interface recombination velocities at the first and second interfaces, respectively. R_1 is the reflectivity of the front surface and R_2 and R_3 are the effective reflectivities at the two interfaces, respectively. P and $h\nu$ are the power and the photon energy of the incident laser beam. η is the quantum yield, which is the optical-to-electrical energy conversion efficiency.

APPENDIX B: PCR SIGNAL EXPRESSIONS FOR SAMPLE OF SINGLE HOMOGENEOUS LAYER

The PCR signal for the single layer model follows:

$$S_{\text{PCR-}S}(\omega)=C\int_0^\infty \tilde{F}_S(\delta,\omega)J_1(\delta w)\,d\delta, \tag{B1}$$

with

$$\tilde{F}_S(\delta,\omega)=\frac{1-\exp(-\beta L)}{\beta}[A+B\exp(\beta L)] + \frac{E}{\alpha}[1-\exp(-\alpha L)]. \tag{B2}$$

Where

$$\beta^2=\delta^2+\frac{1+i\omega\tau}{D\tau}, \tag{B3}$$

$$E=\frac{\alpha(1-R)\eta P}{2\pi h\nu D}\frac{\exp(-\delta^2 a^2/4)}{\beta^2-\alpha^2}, \tag{B4}$$

$$A=-\frac{1}{H}[a_2 b_1\exp(\beta L)-a_1 b_2\exp(-\alpha L)]E, \tag{B5}$$

$$B=-\frac{1}{H}[b_1\exp(-\beta L)-b_2\exp(-\alpha L)]E, \tag{B6}$$

$$H=a_2\exp(\beta L)-a_1\exp(-\beta L); \tag{B7}$$

$$a_1=\frac{D\beta-s_1}{D\beta+s_1}, \tag{B8}$$

$$b_1=\frac{D\alpha+s_1}{D\beta+s_1}, \tag{B9}$$

$$a_2=\frac{D\beta+s_2}{D\beta-s_2}, \tag{B10}$$

$$b_2=\frac{D\alpha-s_2}{D\beta-s_2}, \tag{B11}$$

Here, D and τ are the minority carrier diffusion coefficient and lifetime of the sample, and α and L are its absorption coefficient and thickness, respectively. s_1 and s_2 are the front and rear surface recombination velocities of the sample, respectively. R is the reflectivity of the front surface. The definitions of other symbols are the same as in Appendix A.

[1] A. Mandelis, J. Batista, and D. Shaughnessy, Phys. Rev. B **67**, 205208 (2003).
[2] A. Mandelis, R. Bleiss, and F. Shimura, J. Appl. Phys. **74**, 3431 (1993).
[3] A. Mandelis, A. Othonos, C. Christofides, and J. Boussey-Said, J. Appl. Phys. **80**, 5332 (1996).
[4] A. Salnick, A. Mandelis, and C. Jean, Appl. Phys. Lett. **69**, 2522 (1996).
[5] A. Salnick, A. Mandelis, H. Ruda, and C. Jean, J. Appl. Phys. **82**, 1853 (1997).
[6] T. Ikari, A. Salnick, and A. Mandelis, J. Appl. Phys. **85**, 7392 (1999).
[7] M. E. Rodríguez, A. Mandelis, G. Pan, J. A. García, V. Gorodokin, and Y. Raskin, J. Appl. Phys. **87**, 8113 (2000).
[8] D. Shaughnessy and A. Mandelis, J. Appl. Phys. **93**, 5236 (2003).
[9] D. Shaughnessy and A. Mandelis, J. Appl. Phys. **93**, 5244 (2003).
[10] M. E. Rodriguez, A. Mandelis, G. Pan, L. Nicolaides, J. A. Garcia, and Y. Riopel, J. Electrochem. Soc. **147**, 687 (2000).
[11] A. Schoenecker, J. A. Eikelboom, A. R. Burgers, P. Loelgen, C. Leguijt, and W. C. Sinke, J. Appl. Phys. **79**, 1497 (1996).
[12] B. Li, D. Shaughnessy, A. Mandelis, J. Batista, and J. Garcia (unpublished).
[13] Ch. Wilbertz, K. L. Bhatia, W. Kraetschmer, and S. Kalbitzer, Mater. Sci. Eng., B **2**, 325 (1989).
[14] A. Salnick and J. Opsal, J. Appl. Phys. **91**, 2874 (2002).
[15] G. Popescu and I. Boca, Thin Solid Films **233**, 207 (1993).
[16] M. Fried and Redei, Thin Solid Films **364**, 64 (2000).
[17] *Handbook of Optical Constants of Solids*, edited by E. D. Palik, Vols. I and III (Academic, San Diego, 1998).
[18] J. Batista, A. Mandelis, and D. Shaughnessy, Appl. Phys. Lett. **82**, 4077 (2003).
[19] A. W. Stephens and M. A. Green, J. Appl. Phys. **80**, 3897 (1996).
[20] A. Pinto Neto, H. Vargas, N. F. Leite, and L. C. M. Miranda, Phys. Rev. B **41**, 9971 (1990).
[21] D. K. Schroder, *Semiconductor Material and Device Characterization*, 2nd ed. (Wiley, New York, 1998), Chap. 7.4.
[22] K. L. Luke and L. J. Cheng, J. Appl. Phys. **61**, 2282 (1987).